Optics Letters

Quasi-rhombus metasurfaces as multimode interference couplers for controlling the propagation of modes in dielectric-loaded waveguides

Chaonan Yao,[1,2] Subhash C. Singh,[1,2,3,4] Mohamed ElKabbash,[3] Jihua Zhang,[3] Huanyu Lu,[1,2] and Chunlei Guo[1,2,3,*]

[1]Guo Photonic Laboratory, Changchun Institute of Optics, Fine Mechanics and Physics, Chinese Academy of Science, Changchun 130033, China
[2]University of Chinese Academy of Science, Beijing 100039, China
[3]The Institute of Optics, University of Rochester, Rochester, New York 14627, USA
[4]e-mail: ssingh49@ur.rochester.edu
*Corresponding author: guo@optics.rochester.edu

Received 2 January 2019; revised 15 February 2019; accepted 21 February 2019; posted 21 February 2019 (Doc. ID 356277); published 22 March 2019

Metasurfaces can control the propagation of free space and guided modes by imparting a phase gradient and modifying the mode propagation properties. Here we propose a design to control optical signals in a dielectric-loaded waveguide using quasi-rhombus gradient plasmonic metasurface structure. The metasurface acts as a multimode interference coupler that can focus, route, and split the propagating field in UV-visible spectral range. The ability to gain full control on waveguided mode with minimal footprint can significantly impact miniaturization of optical devices and photonic integrated circuits.

https://doi.org/10.1364/OL.44.001654

UV-visible spectroscopic techniques are routinely used to measure properties of materials, growth rate of bio-species, kinetics of chemical reactions, and so on [1–3]. The miniaturization of optical elements has recently become a main driving force in modern photonics to gain full control over light propagation with minimal footprint. High-density photonic integrated circuits (PICs) have the capability to miniaturize bulkier optical devices to chip scale to make them available at an affordable cost to the public for immediate point of medical care, e.g., for cancer imaging [4]. Furthermore, the demand to increase the packing density of PICs while minimizing the overall power consumption necessitates more compact optical elements [5]. However, photonic circuits and systems are facing several challenges, including difficulties in miniaturization, low optical bandwidth, high insertion losses, and lack of a knob to control propagation and steering of optical modes into different optical interconnects. Therefore, it is highly desirable to design waveguides, an important component of PICs, with low losses and high performance in the UV-visible spectral region with added functionality to control propagation, steering, and coupling of optical systems into different optical interconnects.

Multimode interference (MMI) couplers are widely used photonic devices that can act as an efficient optical splitters or combiners over a wide wavelength range, with weak sensitivity to polarization and dispersion [6]. However, MMI couplers have an additional element that connects n input fibers with m output fibers, which means that they have a sizeable footprint.

The miniaturization of optical elements has been revolutionized after the introduction of metasurfaces—two-dimensional antenna arrays that impart an abrupt phase change on propagation [7] or guided [8] electromagnetic (EM) modes. In particular, introducing a gradient antenna array on a waveguide can provide additional momentum components to the guided mode, thus modifying the guided mode order. The ability to do so means that MMI couplers can be crafted from metasurfaces overlaid on a waveguide, i.e., without introducing a separate coupler.

Here, we designed a dielectric loaded waveguide (DLW) [9] with quasi-rhombus plasmonic metasurface as an MMI coupler to condense, steer, and bend guided modes. Light propagating in the DLW, patterned with gradient metasurface is self-imaged periodically due to the generation of higher-order guided modes. The self-image can be focused and coupled to a narrower waveguide in a 1×1 configuration or to a specific output waveguide in a 1×2 configuration [10,11]. The designed metasurface completely removes the requirement for tapers or couplers, hence, reducing the overall length of the optical system and associated losses. Thus, the designed metasurface on DLW has the capability to realize high-density PIC for fabrication of miniaturized UV-visible optical devices for biomedical diagnosis.

A DLW is designed with an alumina ridge ($h_1 = 200$ nm) on the surface of aluminum ($h_2 = 100$ nm) film deposited on

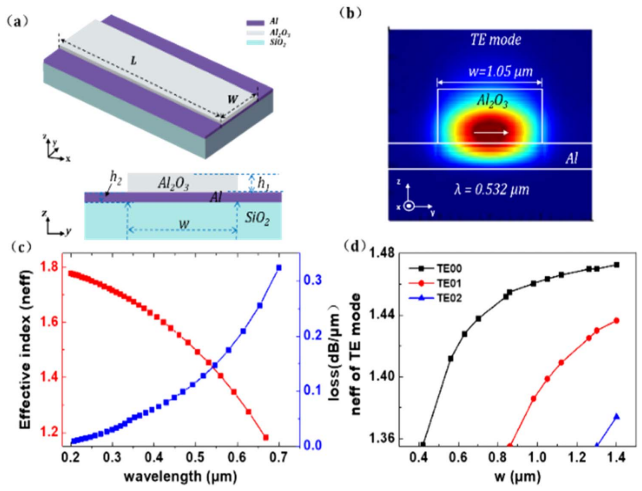

Fig. 1. (a) Schematic illustration of DLW without metasurface (b) calculated mode profile in a DLW for 1.05 μm width. The density plot shows power in the propagation direction for TE_{00} mode at the indicated wavelength, while the arrows represent the in-plane intensity and orientation of the electric field. (c) Effective index as function of wavelength and corresponding loss. (d) Dependence of the real part of the effective index for TE_{00}, TE_{01}, and TE_{02} modes on the width of the DLW waveguide at λ=0.532μm with h_1 = 200 nm and h_2=100nm.

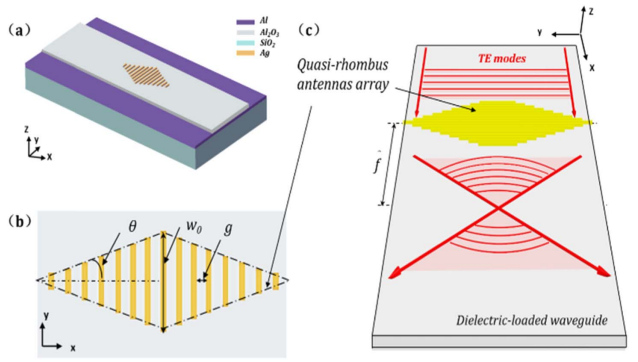

Fig. 2. (a) Schematic illustration of DLW with the structure of MMI, a quasi-rhombus antennas array. (b) The quasi-rhombus metasurfaces consist of silver antennas (yellow rods) patterned on DLW surface. The DLW includes Al_2O_3 layer and Al layer on SiO_2 substrate. The length (w) of antenna first increases up to the maximum length (w_0) and then decreases successively. (c) The interference of TE modes, located in the transmission region, depends only on the geometrical parameters of quasi-rhombus metasurface: g (gap between two nanorods) and θ, which depends on rate, dw/dx, of change in the length of antenna with distance and w_0 (length of the longest nanorod).

a glass substrate [Fig. 1(a)]. The permittivity of alumina and aluminum are calculated following the Drude model and directly used in finite-difference-time-domain (FDTD) simulation (Lumerical Inc.). In order to achieve the highest localization of field for dielectric mode at its maximal propagation length, we optimize width for the DLW, and based on the obtained mode profile, w = 1.05 μm is selected as the most suitable width. Propagation loss is calculated using the imaginary part of the modal effective index with an assumption that only fundamental mode of the EM field propagates in DLW [9]. Figure 1(b) presents the mode profile of optical signal (λ = 0.532 μm) propagating in a DLW of 1.05 μm width. Spectral variation in the real part of the effective index and corresponding loss (dB/μm) for 1.05 μm wide DLW is shown in Fig. 1(c). The dependence of effective indices on the width of DLW for TE_{00}, TE_{01}, and TE_{02} modes at 0.532 μm wavelength is presented in Fig. 1(d). The fundamental TE_{00} mode exists for any width larger than 0.4 μm, while higher-order modes emerge as the width of DLW increases. The cutoff widths for TE_{00}, TE_{01}, and TE_{02} modes are ~400 nm, 830 nm, and 1300 nm, respectively [Fig. 1(d)]. It means that the width of DLW controls the types of modes allowed to propagate.

A gradient metasurface structure, designed on the surface of DLW, acts as an MMI coupler that enables coupling of waveguide modes as a consequence of their interaction with metasurfaces [8,12]. The gradient metasurfaces introduce a phase gradient, equivalent to an effective wavevector, along the surface and control guided waves by strong, consecutive scattering events at the antenna array [8]. The designed gradient metasurface structure consists of a quasi-rhombus array of silver nanorod antennas patterned on the top surface of a DLW [Fig. 2(a)]. Indices of Ag are obtained by interpolating values measured by Johnson and Christy [13]. The antennas are periodically distributed and symmetrically located with respect to the central slit. These antennas are arranged in such a way that their assembly looks like a convex lens facing the incident plane wave [Figs. 2(b) and 2(c)]. The gradient metasurface is designed from a periodic array of silver nanorods. The length of the rod successively increases with a rate dw/dx, where w is the length of the silver nanorod, attaining maximum length, w_0, and successively decreasing to make a symmetrical pattern [Figs. 2(b) and 2(c)]. The rate of change in the length of the antenna introduces a phase gradient $d\varphi/dx$ that is equivalent to effective wavevector Δk along the surface [8,12]. The change in the effective wavevector Δk causes refraction at each point of plane wave-front and condenses EM field to produce a first-fold image. The first-fold image produced with the designed quasi-rhombus metasurface structure is very similar to the focal point of an optical system with finite aperture [Fig. 3(a)] [14]. We performed FDTD simulations to calculate the near-field electric field (E-field) distributions and compare the results with the theoretical self-imaging property in the designed MMI structures. Perfect matched layer (PML) boundary conditions are used at the three boundaries. Employing the effective index method, we calculated the effective propagation indices and propagation lengths of the guided modes supported by the MMI waveguide as a function of width of the DLW.

The incident TE fundamental waveguide mode depends on the design parameters, which include the phase gradient (g and θ), array length, and offset (s) of the antenna array from the waveguide center. Figure 3 shows the E-field profile for fundamental mode propagating from left to right in DLW with quasi-rhombus metasurfaces. The TE mode for the input of DLW is excited by a mode source with a central wavelength λ = 0.532 μm. In Fig. 3(a), we notice that the E-field profile of the fundamental TE mode couples with higher-order modes when MMI structure is used. Here, metasurface structure focuses incident TE mode at the focus through MMI, and the E-field profile at the focus is self-imaged following the self-imaging (SI) principle. In SI, the input field profile reproduces single or multiple images of its own at a periodic interval

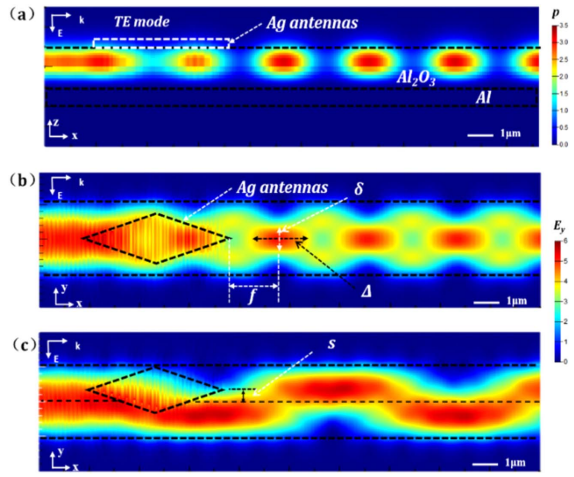

Fig. 3. Optical power transmission in waveguides patterned with gradient metasurfaces. (a) Spatial distribution of the magnitude of the Poynting vector (x-z view), showing highly asymmetric optical power flow as a result of the directional mode conversion. E_y field intensity (x-y view) profile (arbitrary units) for the case $\theta = 8.5°$, $w_0 = 800$ nm, and $g = 0.25$ μm for (b) $s = 0$ (no offset) and (c) $s = 0.2$ μm. Operating wavelength (λ) is 0.532 μm in all cases from (a) to (c).

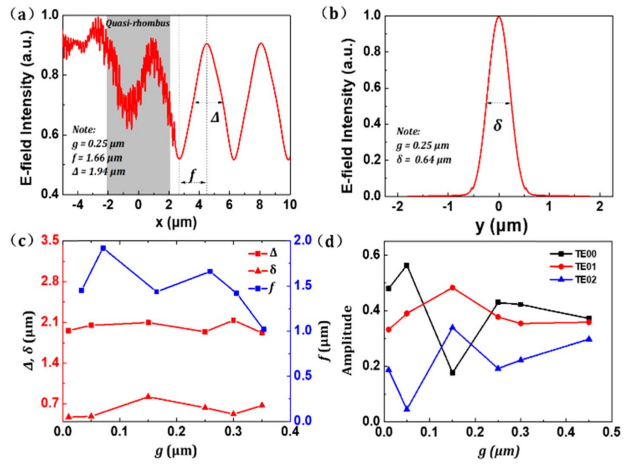

Fig. 4. Focusing light with the quasi-rhombus antennas array on the DLW. (a) Variation in electric field profile with length of propagation (x) at $y = 0$ μm. (b) Variation in electric field profile at first focus $x = 4.21$ μm (c) Curves for the geometrical parameters after the MMI structure by defining the focus (f, Δ, and δ) as a function of g. (d) Amplitudes of different modes (mode purity) at the center of one-fold image as a function of gap distance, g, between two nanorods.

L along the propagation axis following the respective conditions of $L = p(3L_\pi)$ or $L = p/2(3L_\pi)$, where L_π is the beat length of the two lowest-order modes, and p is a constant [14]. This is caused mainly by the strong crosstalk between Ag antennas. Figures 3(a) and 3(b) show the optical power (x-z view) and field distribution of E_y (x-y view) at the center of the alumina layer when the fundamental TE mode is launched using MMI structure. Figure 3(c) shows simulations of mode evolution when light propagates from the left to the right through a region of the waveguide patterned with the quasi-rhombus structure with its longer axis offset by $s = 0.2$ μm from the center of the waveguide. Since DLW with gradient metasurfaces rely on the SI principle, high-order modes propagate with 0.2 μm offset from the waveguide center. In Fig. 3(c), it is interesting to note that the designed metasurface on DLW can be used for sharp bending of waveguide modes through its offset or inclined orientation from the propagation axis of DLW.

SI quality refers to how accurately the input field is reproduced at the end of the MMI structure. According to Fig. 3(b), there are onefold, twofold, and threefold images at three different points. By looking at the far-field region, for $g = 0.25$ μm, a highly collimated beam with a very low divergence is observed, but also it is worth commenting on the appearance of an elongated focus at around $x = 4.21$ μm [Fig. 4(a)]. From the SI principle [14,15], it is expected that the onefold, twofold, and threefold images occur at the distances $x_1 = 4.21$ μm, $x_2 = 7.86$ μm, and $x_3 = 11.51$ μm, respectively. Clearly, there is an approximate focusing effect associated with the beaming phenomenon [see schematic in Fig. 2(c)]. Up to this point, we have discussed only first-order imaging. Let us now concentrate on the properties of this focus (i.e., onefold imaging) for the wavelength at which beaming is maximum.

In Fig. 4, we present the spatial profile of E-field distribution in detail by extracting E-field intensity from Fig. 3(b) along the line $y = 0$ [Fig. 4(a)] and by the line of maximum e-field intensity at first focus $x = 4.21$ μm [Fig. 4(b)]. These curves also help us to further characterize the focus by defining the focal length (f), focal depth (Δ, full width at half-maximum of E-field intensity of the first-fold image along the x direction), and focal width (δ, as before, but this time along the y direction). Here the focal spot is of elliptical shape, and Δ and δ are dimensions for longer and shorter axes of the ellipse. The focal length is the distance to the surface of E-field intensity of the onefold image, instead of L_π to characterize the performance of imaging. We have found that for a given combination of θ and w_0 values, there is a g that gives the resonant wavelength (λ_R). Figure 4(c) presents the g dependence of the geometrical characteristics of the first focus: f, Δ, and δ. These curves demonstrate that focal length of MMI structure has strong dependence, while focal depth and width are weak functions of g. Some of the guided modes in the multimode waveguide are excited only by the input field. Figure 4(d) shows that there are three mode inferences. The ratios of the three modes vary with gap distance. This is because the quasi-rhombus metasurfaces introduce mode phase factor to adjust MMI in DLW.

PIC generally uses tapers to couple optical signal from wide to narrow waveguides, which significantly increases length of overall waveguides and hence increase associated losses. Figure 5 shows FDTD simulations for two modes' evolutions in DLW when light propagates from left to the right through a region of the waveguide patterned with the gradient metasurfaces. In Figs. 5(a1)–5(a3), we show that TE modes in a 1.05 μm wide DLW can be condensed and hence efficiently coupled into a narrower, 400 nm wide, waveguide through a MMI structure. Design parameters (w_0, θ, and g) for MMI structure control the coupling coefficient at a given wavelength. Compared with waveguide tapers, the transmission of the DLW with MMI structure is higher in the wavelength range of 450–530 nm [Fig. 5(a3)].

For the MMI power splitters, the TM modes supported by a wide silicon-on-insulator (SOI) waveguide can be split into several narrow hybrid plasmonic (HP) waveguides through an HP MMI [15]. The splitting and routing of a beam using quasi-rhombus

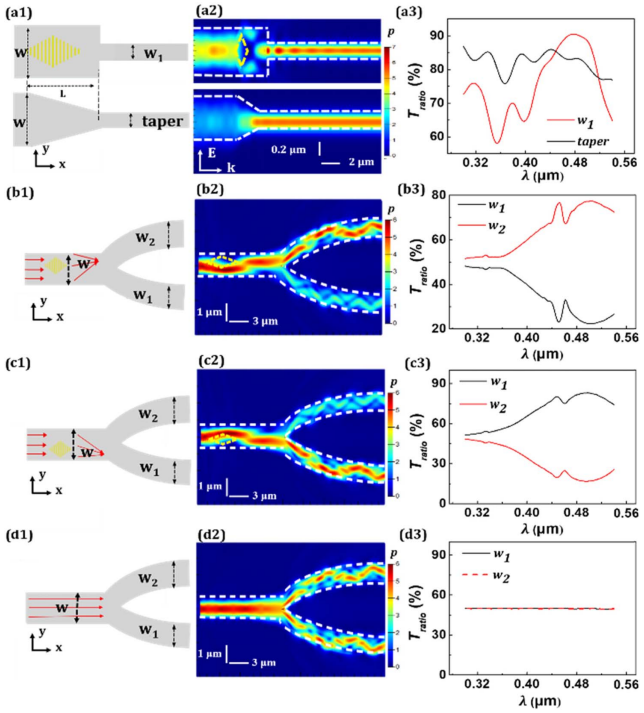

Fig. 5. Beam splitting and routing via the quasi-rhombus structure in DLWs. Two representative designs for (a1) wide to narrow waveguide coupling, where $w = 1.05$ μm, $w_1 = w_{taper} = 400$ nm, $w_0 = 0.8$, $g = 10$ nm, and $L = 2$ μm. (b1) Waveguide splitter. (a2), (b2) Corresponding simulation results of electric field intensity profiles at $\lambda = 0.532$ μm. (a3) Spectral distribution of T_{ratio} at the centers of wide and narrow waveguides shown in (a1) and compared with traditional waveguide taper; (b3) two branches w_1 and w_2 shown in (b1). (d1) Waveguide splitter, same as (c1), without the MMI structure. In (b1), (c1), and (d1), $w = w_1 = w_2 = 1.05$ μm, $w_0 = 0.6$ μm, $g = 250$ nm, and $s = 0.2$ μm. (b2), (c2), and (d2) are corresponding simulations showing that the bending of light is off the optical axis. (c3), (d3) Spectral distribution of T_{ratio} at centers of w_1 and w_2 in DLWs shown in (c1) and (d1), respectively.

metasurfaces depends on the phase gradient, array length, offset of the antenna array from the waveguide center, and width. Figures 5(b1) and 5(c1) show MMI structures designed on the surface of DLW with $s = +0.2$ μm and $s = -0.2$ μm, respectively, from its axis. Figures 5(b2) and 5(c2) show corresponding E-field intensity profiles at $\lambda = 0.532$ μm in Y-shaped DLW for the given geometrical parameters of MMI structures. Figures 5(b3) and 5(c3) show that the emission intensity at the two output ends of the Y-shaped branch structure is dependent on the offset of the antenna array from the waveguide center. Compared with a balanced power splitting (1 : 1), shown in Fig. 5(d2), more power is transmitted to one of the two side waveguides by moving the quasi-rhombus antennas array in Figs. 5(b2) and 5(c2). As seen in Fig. 5, the quasi-rhombus structures not only control bending angle, but also control light distribution and intensity.

We measured the ratio of transmission passing among the output waveguides in Figs. 5(a3), 5(b3), and 5(c3), which is an important parameter to characterize the performance of an MMI power splitter. Here the ratio of transmission is defined as $T_{ratio} = P_{out}/P_{in}$, where P_{out} and P_{in} are powers at output and input of DLW, respectively. We observe that the T_{ratio} is significantly higher than 75% at $\lambda = 0.532$ μm in Fig. 5(b3). For Y-shaped power splitters, we can control the magnitude of powers by changing position of quasi-rhombus metasufaces. We can get a particular T_{ratio} of each side waveguide by adjusting the s in Fig. 5. Thus, an intuitive approach to improve the efficiency of splitting does not only depend on the phase gradient and array length but also on the distance between quasi-rhombus metasufaces and side of the waveguide, which causes different energy to decouple into DLW and propagate to the far field.

In summary, we have designed a new knob, quasi-rhombus metasurfaces to achieve the function of an MMI on DLWs in the UV-visible region. We have analyzed theoretically the geometrical parameters of finite arrays of antennas that are equally spaced. The TE modes in a 1.05 um wide DLW can be directly coupled into a 400 nm wide waveguide by adjusting geometrical parameters of a quasi-rhombus metasurface. The quasi-rhombus matesufaces not only control the bending angle, but also light distribution and intensity as a knob of PIC. These MMI structures may have valuable applications in designing universal logic, NAND and NOR, gates [16]. With these advantages, we expect that our quasi-rhombus metasurfaces will advance high-density PICs for miniaturization of UV-visible optical devices for biomedical diagnosis and other applications.

Funding. National Key Laboratory of Science and Technology on Communications (2017YFB1104700); National Natural Science Foundation of China (NSFC) (11674178, 11774340); Natural Science Foundation of Jilin Province (20180414019GH); Scientific Research Project of the Chinese Academy of Sciences (CAS) (QYZDB-SSW-SYS038).

REFERENCES

1. E. Segev, J. Reimer, L. C. Moreaux, T. M. Fowler, D. Chi, W. D. Sacher, M. Lo, K. Deisseroth, A. S. Tolias, A. Faraon, and M. L. Roukes, Neurophotonics **4**, 011002 (2016).
2. A. N. Zorzos, J. Scholvin, E. S. Boyden, and C. G. Fonstad, Opt. Lett. **37**, 4841 (2012).
3. J. N. Anker, W. P. Hall, O. Lyandres, N. C. Shah, J. Zhao, and R. P. VanDuyne, Nat. Mater. **7**, 442 (2008).
4. T. Imamura, T. Saitou, and R. Kawakami, Cancer Sci. **109**, 912 (2018).
5. Y. Fang and M. Sun, Light: Sci. Appl. **4**, e294 (2015).
6. P. E. Morrissey, H. Yang, R. N. Sheehan, B. Corbett, and F. H. Peters, Opt. Commun. **340**, 26 (2015).
7. N. Yu, P. Genevet, M. A. Kats, F. Aieta, J.-P. Tetienne, F. Capasso, and Z. Gaburro, Science, **334**, 1210713 (2011).
8. Z. Li, M.-H. Kim, C. Wang, Z. Han, S. Shrestha, A. C. Overvig, M. Lu, A. Stein, A. M. Agarwal, M. Lončar, and N. Yu, Nat. Nanotechnol. **12**, 675 (2017).
9. M. Hano, IEEE Trans. Microwave Theory Tech. **32**, 1275 (1984).
10. Z. Han and S. He, Opt. Commun. **278**, 199 (2007).
11. G. Yuan, P. Wang, Y. Lu, and H. Ming, Opt. Express **17**, 12594 (2009).
12. N. Yu and F. Capasso, Nat. Mater. **13**, 139 (2014).
13. P. B. Johnson and R. W. Christy, Phys. Rev. B **6**, 4370 (1972).
14. L. B. Soldano and E. C. M. Pennings, J. Lightwave Technol. **13**, 615 (1995).
15. S. Yi, W. Jing, Y. Min, and Q. Min, J. Opt. **13**, 075002 (2011).
16. H. Wei, Z. Wang, X. Tian, M. Käll, and H. Xu, Nat. Commun. **2**, 387 (2011).